Self-supported Co-doped FeNi carbonate hydroxide nanosheet array as a highly efficient electrocatalyst towards the oxygen evolution reaction in alkaline solution

Yu-Feng Qi,[a] Qian Wang,[a] Xiu-Guang Wang,[a] Zheng-Yu Liu,[a] Xiao-Jun Zhao*[a,b] and En-Cui Yang*[a]

Reagents: All initial reagents were commercially purchased and used without further purification. Hydrochloric acid was supplied by Fengchuan Chemical Reagent Science and Technology Co., Ltd (Tianjin, China). $Fe(NO_3)_3·9H_2O$ and ethyl alcohol were obtained from Aladdin Ltd (Shanghai, China). $Co(NO_3)_2·6H_2O$, $Ni(NO_3)_2·6H_2O$, urea and NH_4F were from Macklin Biochemical Co., Ltd (Shanghai, China). KOH was given by Rhawn reagent Co., Ltd (Shanghai, China). Deionized water purified by a Millipore system was used during the whole experiments. Nickel foam (NF) was purchased from Chemart Chemical Technology Co., Ltd (Tianjin, China).

Pre-treatment of NF: A piece of NF with the dimensions of 3.0 cm ×3.0 cm×1.5 mm was sonicated in 2.0 M HCl solution for 15 min to get rid of the superficial NiO_x layer. Then, it was sonicated in water for 15 min and subsequently washed with ethanol three times to ensure the surface of the NF clean. Lastly, the NF was dried in vacuum oven at 60 ^oC for 4 h and the weight of the well-treated NF was recorded precisely.

Preparation of Co-FeNi CH/NF: A mixture containing 0.6 mmol of $Fe(NO_3)_3·9H_2O$, 0.6 mmol of $Co(NO_3)_2·6H_2O$, 0.6 mmol of $Ni(NO_3)_2·6H_2O$, 8.0 mmol of NH_4F and 10.0 mmol of urea was dissolved in 40.0 mL deionized water and magnetically stirring for 15 min to form a clear solution. Then, the obtaining solution was transferred into a 50.0 mL Teflon-lined stainless-steel autoclave with a piece of pre-treated NF (3.0 cm × 3.0 cm × 1.5 mm) placed vertically in it. The autoclave was heated to 120 ^oC and kept at 120 ^oC for 10 hours. After the autoclave was cooled to room temperature naturally, the NF coated with the as-synthesized solid was taken out from the autoclave and washed with deionized water for 5 times to remove the non-tight integrating powder and dried at 60 ^oC in vacuum for 24 hour. The mass loading of the catalyst is about 3.0 mg cm^{-2} measured precisely by Sartorius BSA124S electronic balance (0.1 mg).

Preparations of FeCo CH/NF, FeNi CH/NF and CoNi CH/NF: Bimetallic FeCo CH/NF, FeNi CH/NF and CoNi CH/NF were respectively synthesized according to the same procedures mentioned above only with the corresponding metal salts as initial materials. The mass loadings of the catalysts were 3.1, 3.0 and 3.2 mg cm^{-2} for FeCo CH/NF, FeNi CH/NF and CoNi CH/NF, respectively.

Characterizations: Infrared spectrum data was collected on a Thermo Scientific Nicolet iS 50 FT-IR spectrometer. Crystalline phases of the samples were identified on a Bruker D8 advance diffractometer at 60 kV and 300 mA for a Cu *K*α radiation (λ = 1.5406 Å) with a scan speed of 0.2° min^{-1} and a step size of 0.02° in 2θ. The morphology of the samples were observed by a field emission scanning electron microscopy (FE-SEM, Nova Nano 230, FEI) at an accelerating voltage of 10 kV and a field emission transmission electron microscopy (FE-TEM, G^2 F20, FEI) with an accelerating voltage of 200 kV. Energy-dispersive X-ray spectra (EDS) and selected area electron diffraction (SAED) were respectively performed on the SEM and TEM. X-ray photoelectron spectroscopy (XPS) measurements were performed on an AXIS $ULTRA^{DLD}$ X-ray photoelectron spectrometer (Kratos) with a Al Kα radiation. Binding energies of XPS spectra were calibrated relative to the C 1s peak (284.6 eV) from hydrocarbons adsorbed on the surface of samples.

Electrochemical measurements: Electrochemical measurements were carried out on an electrochemical working station (CHI 660E, Shanghai) in a standard three-electrode system. As-prepared catalyst was employed as working electrode, graphite rod (CHI Inc. China) and Ag/AgCl (KCl saturated) were respectively used as as counter electrode and reference electrode in 1.0 M KOH solution. The Ag/AgCl reference electrode was calibrated before and after each experiment.[1] The OER catalytic activity was investigated using linear sweep voltammetry (LSV) at a scan rate of 5.0 mV s^{-1} in O_2-saturated KOH solution with 90% *iR*-compensation. To minimize the influence of multiple redox peaks caused by the valence change of metal ions between 1.2 and 1.4 V, a reverse scan mode was adopted by setting the voltage scale from 0.8 V to 0 V (versus Ag/AgCl).[2-4] A number of cyclic voltammetry (CV) scans have been carried out to stabilize the electrode prior to LSV measurements (Fig. S6). The Tafel slope was calculated from the Tafel equation: $\eta = b\log j + a$, where j is the current density, a is the constant and b is the Tafel slope. The double layer capacitance, which is positive related with the electrochemical surface area (ECSA), was measured by CV in the non-faradaic region of the voltammogram at different scan rates of 1.0, 2.0, 3.0, 4.0 and 5.0 mV s^{-1}. Electrochemical impedance spectroscopy (EIS) was measured in a frequency range from 100 kHz to 0.1 Hz at the amplitude of the sinusoidal voltage of 5.0 mV. The durability test of the electrocatalyst was carried out using the potentiostatic electrolysis at a fixed potential without *iR*-correction. Turnover frequency (TOF) value of the electrocatalyst was calculated from the equation TOF =

$j \times A / 4 \times n \times F$, where j was the current density obtained at a given overpotential in A cm^{-2}, A was the surface area of the electrode, 4 stands for the number of transferred electron in oxygen evolution reaction, F is Faraday's constant with a value of 96485.3 C mol^{-1}, and n represents the mole number of active sites of the catalyst. Herein, we assume that all the metal ions are active sites, and n is calculated by the loading weight and relative weight of metal ions of the catalysts. All the potentials reported herein were calibrated with respect to the reversible hydrogen electrode (RHE) using the following Nernst equation $E_{RHE} = E_{Ag/AgCl} + 0.197 + 0.059 \times pH$ unless stated otherwise. The overpotential (η) was calculated using the formula, η (V) = E (RHE) – 1.23 V.

Fig. S1 Photographs of the as-synthesized samples (a: bare NF, b: FeCo CH/NF, c: CoNi CH/NF d: FeNi CH/NF and e: Co-FeNi CH/NF).

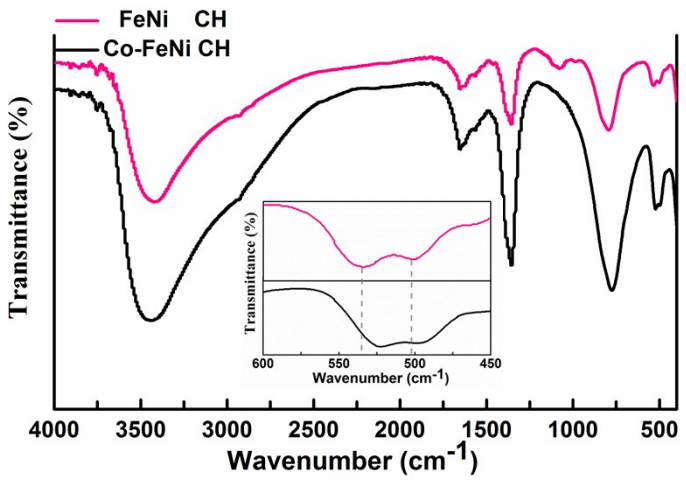

Fig. S2 FT-IR spectra of Co-FeNi CH and FeNi CH.

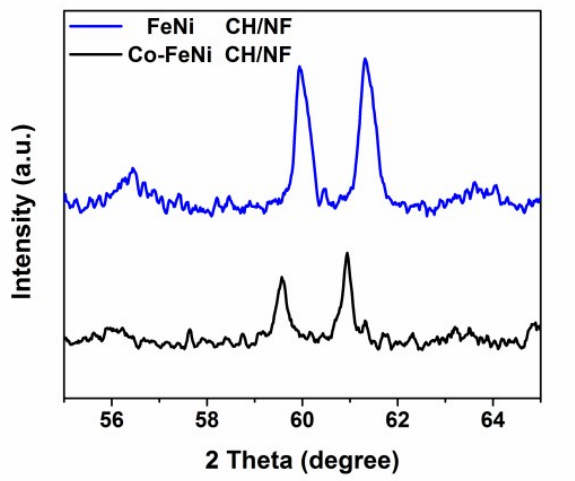

Fig. S3 Comparisons of XRD patterns of Co-FeNi CH/NF and FeNi CH/NF.

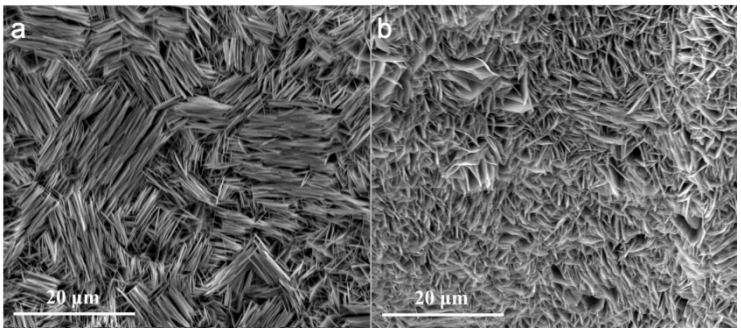

Fig. S4 SEM images of FeNi CH/NF (a) and Co-doped FeNi CH/NF (b).

Table S1 SEM-EDS results of Co-FeNi CH.

Element	*At%*
C	6.22
O	47.49
Si	3.02
Fe	11.22
Co	10.95
Ni	20.90

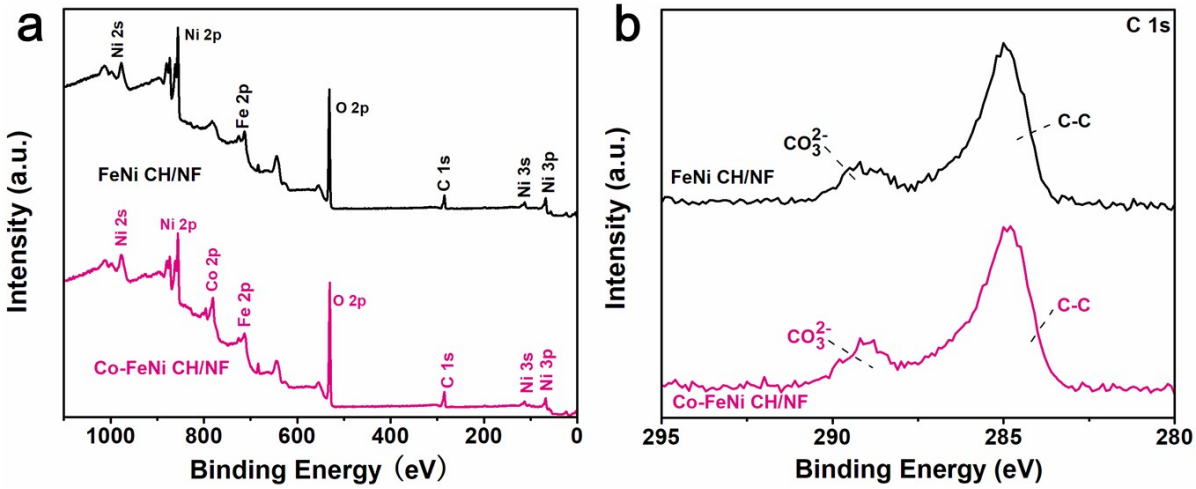

Fig. S5 (a) Overall XPS spectra of Co-FeNi CH/NF and FeNi CH/NF. (b) High-resolution C 1s spectra of Co-FeNi CH/NF and FeNi CH/NF.

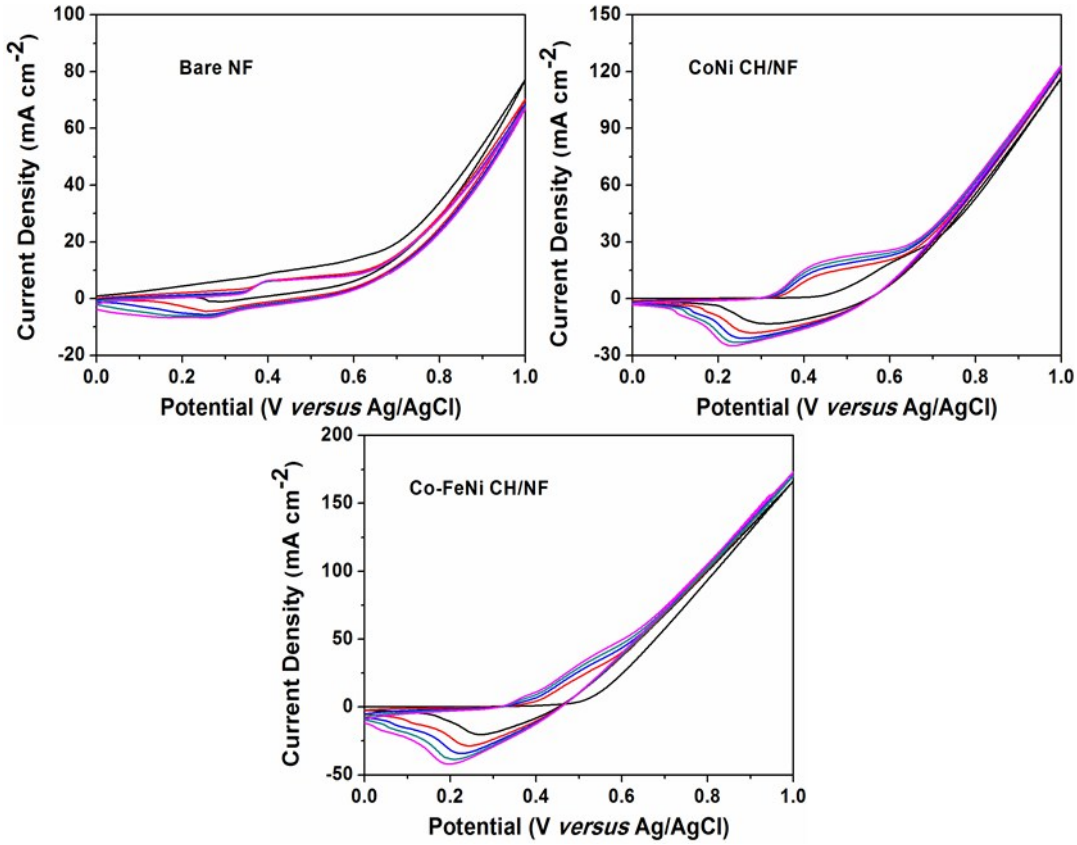

Fig. S6 Activation curves of bare NF, CoNi CH/NF, and Co-FeNi CH/NF by cyclic voltammetry.

Table S2 Comparisons of different self-supported OER catalysts in alkaline solution

Catalyst	Substrate	Loading mass (mg cm^{-2})	η_{10} (mV)	η_{30} (mV)	η_{50} (mV)	Tafel slope (mV dec^{-1})	Ref.
Co-FeNi CH	NF	~3	202			37.5	This work
FeCo CH	NF	~3	230			62.3	This work
FeNi CH	NF	~3	240			61.4	This work
CoNi CH	NF	~3	305			97.7	This work
Co CH	FTO	3.5	466			/	5
$Cu(OH)_2$@CoNi CH NTs	Cu Foam	1.53		288		74	6
Co CH	CP	2.5	240			33	7
Co CH	NF	6	332			126	8
CoMn CH	NF	5.6		294		/	9
FeCH@GDY	NF	/	260			54.5	10
LTHs	CFC	0.4	239			32	11
S-$NiFe_2O_4$	NF	1	267			36.7	12
CoNi$(OH)_x$NTs	Cu Foil	/	280			77	13
NiFeSP	NF	4.2			240	76.3	14

$Ni_xCo_{3-x}O_4$	NF	0.8	337	80	15
P-Co_3O_4	Ti mesh	0.4	280	51.6	16

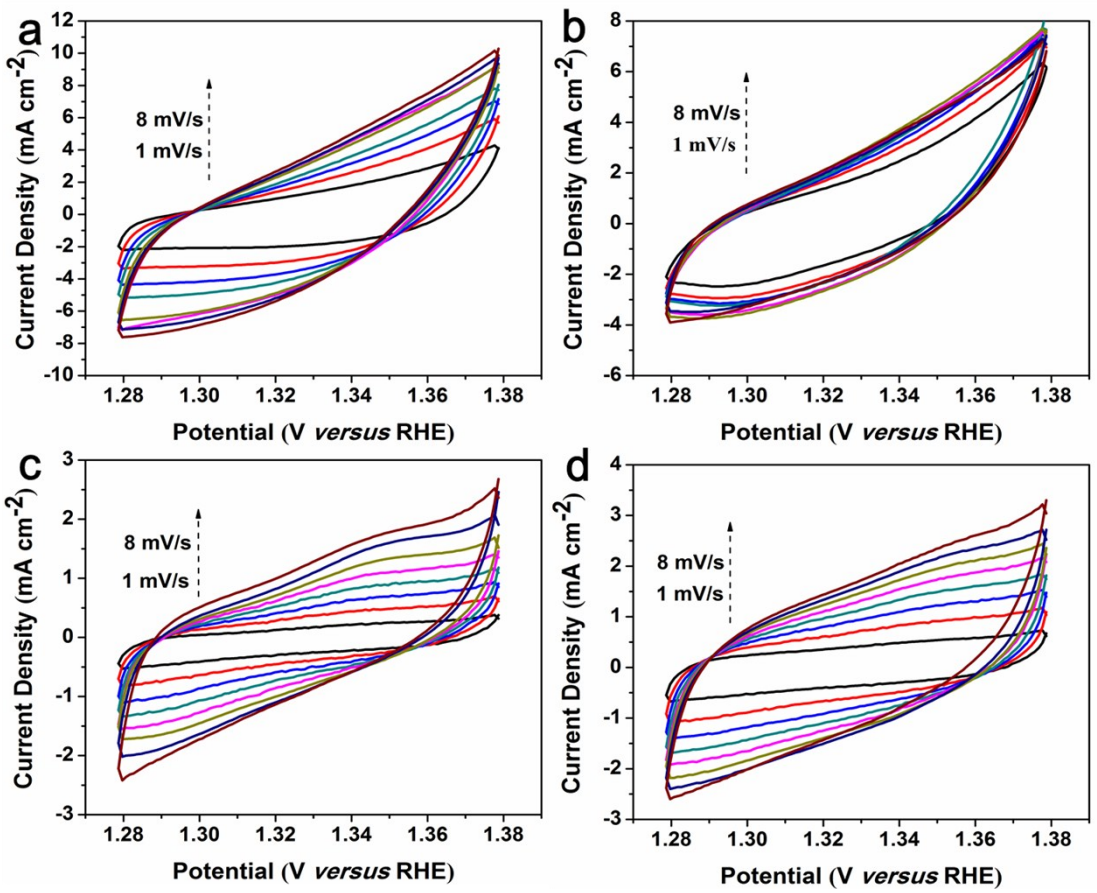

Fig. S7 Scan rate dependence of current densities in CV curves for different electrocatalysts. (a) Co-FeNi CH/NF, (b) FeCo CH/NF, (c) FeNi CH/NF, and (d) CoNi CH/NF.

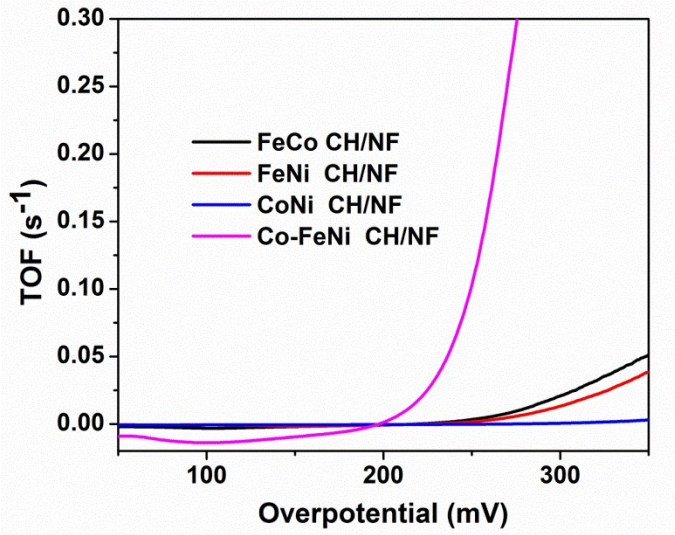

Fig. S8 TOF curves for Co-FeNi CH/NF, FeNi CH/NF, CoNi CH/NF and FeCo CH/NF.

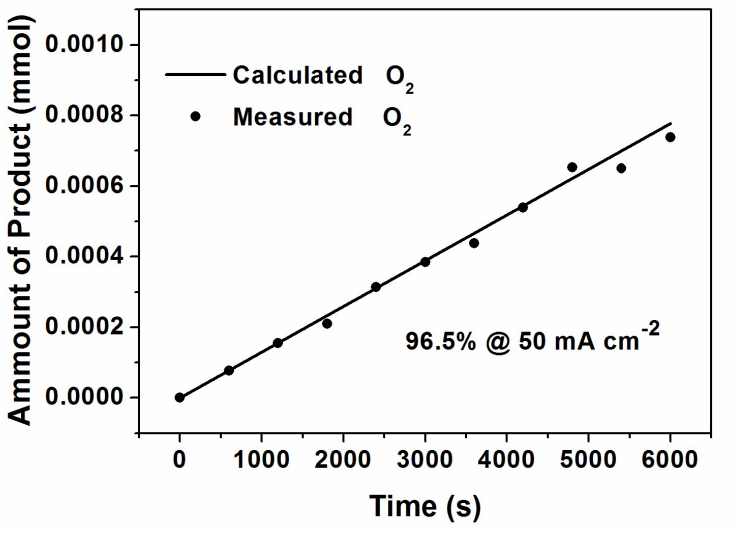

Fig. S9 Current efficiency of Co-FeNi CH/NF sample.

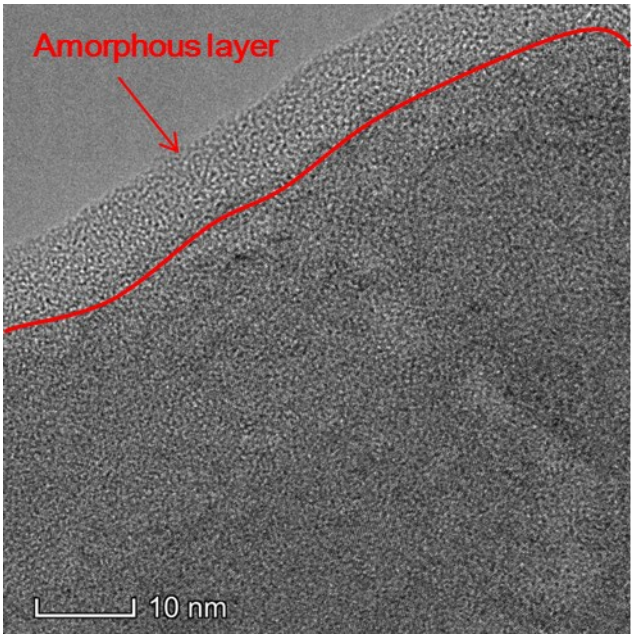

Fig. S10 Amorphous layer observed in Co-FeNi CH/NF after OER by HR-TEM measurement.

Reference

1 Y. Liang, Y. Li, H. Wang, J. Zhou, J. Wang, T. Rigier and H. Dai, *Nature Mater.,* 2011, **10**, 780–786.

2 P. Li, X. Duan, Y. Kuang, Y. Li, G. Zhang, W. Liu and X. Sun, *Adv. Energy. Mater.,* 2018, **8**, 1703341.

3 P. Zhang, L. Li, D. Nordlund, H. Chen, L. Fan, B. Zhang, X. Sheng, Q. Daniel and L. Sun, *Nat. Cummon.*, 2018, **9**, 381.

4 L. Yu, J. F. Yang, B. Y. Guan, Y. Lu and X. W. Lou, *Angew. Chem. Int. Ed.,* 2017, **57**, 172–176.

5 Y. Zhang, B. Cui, O. Derr, Z. Yao, Z. Qin, X. Deng, J. Li and H. Lin, *Nanoscale,* 2014, **6**, 3376–3383.

6 J. Kang, J. Sheng, J. Xie, H. Ye, J. Chen, X. Z. Fu, G. Du, R. Sun and C. P. Wong, *J. Mater. Chem. A,* 2018, **6**, 10064–10073.

7 S. Zhang, B. Ni, H. Li, H. Lin, H. Zhu, H. Wang and X. Wang, *Chem. Commun.,* 2017, **53**, 8010–8013.

8 M. Xie, L. Yang, Y. Ji, Z. Wang, X. Ren, Z. Liu, A. M. Asiri, X. Xiong and X. Sun, *Nanoscale,* 2017, **9**, 16612–16615.

9 T. Tang, W. J. Jiang, S. Niu, N. Liu, H. Luo, Y. Y. Chen, S.F. Jin, F. Gao, L. J. Wan and J. S. Hu, *J. Am. Chem. Soc.,* 2017, **139**, 8320−8328.

10 L. Hui, D. Jia, H. Yu, Y. Xue and Y. Li, *ACS Appl. Mater. Interfaces,* 2019, 11, 2618–2625.

11 A. L. Wang, H. Xu and G. R. Li, *ACS Energy Lett.,* 2016, **1**, 445–453.

12 J. Liu, D. Zhu, T. Ling, A. Vasileff and S. Z. Qiao, *Nano Energy,* 2017, **40**, 264–273.

13 S. Li, Y. Wang, S. Peng, L. Zhang, A. M. Al-Enizi, H. Zhang, X. Sun and G. Zheng, *Adv. Energy Mater.,* 2016, **6**, 1501661.

14 Y. Xin, X. Kan, L. Y. Gan and Z. Zhang, *ACS Nano,* 2017, **11**, 10303−10312.

15 X. Yan, K. Li, L. Lyu, F. Song, J. He, D. Niu, L. Liu, X. Hu and X. Chen, *ACS Appl. Mater. Interfaces,* 2016, **8**, 3208−3214.

16 Z. Xiao, Y. Wang, Y. C. Huang, Z. Wei, C. L. Dong, J. Ma, S. Shen, Y. Li and S. Wang, *Energy Environ. Sci*., 2017, **10**, 2563–2569.